Water Air Soil Pollut (2014) 225:1876
DOI 10.1007/s11270-014-1876-2

# Activated Carbon from Lignocellulosic Waste Residues: Effect of Activating Agent on Porosity Characteristics and Use as Adsorbents for Organic Species

**O. F. Olorundare · T. A. M. Msagati · R. W. M. Krause · J. O. Okonkwo · B. B. Mamba**

Received: 7 September 2013 / Accepted: 15 January 2014 / Published online: 6 February 2014


**Abstract** This paper reports on the effect of activating agents such as the impregnation ratio of phosphoric acid (1:1–1:5) at constant activation temperature on the performance of porous activated carbon from waste residues (maize tassel). The variation in the impregnation ratio of the produced activated carbon (AC) from 1:1 to 1:5 enabled the preparation of a high surface area (1,263 $m^2$/g) and a large pore volume (1.592 $cm^3$/g) of AC produced from maize tassel (MT) using a convectional chemical activating agent (phosphoric acid). Impregnation ratios (IR) of the precursors were varied between 1:1 and 1:5 in which it was found that the ratio of 1:4 was optimal based on the high surface area, while 1:5 has the optimal pore volume value for the produced activated carbon.

**Keywords** Activating agents · Impregnation ratio · Maize tassel · Porous activated carbon

O. F. Olorundare · T. A. M. Msagati (✉) · B. B. Mamba (✉)
Department of Applied Chemistry, University of Johannesburg,
P.O. Box 17011, Johannesburg, South Africa
e-mail: tmsagati@uj.ac.za
e-mail: bmamba@uj.ac.za

R. W. M. Krause
Department of Chemistry, Rhodes University,
P.O. Box 94, Grahamstown 6140, South Africa

J. O. Okonkwo
Department of Environmental, Water & Earth Sciences,
Faculty of Science, Tshwane University of Technology,
Private Bag X680, Pretoria 0001, South Africa

## 1 Introduction

Lignocellulosic wastes generated especially from agricultural wastes have been an issue for environmentalist and eco-friendly activists due to their disposal. Millions of tonnes of wastes generated annually, especially of biomass origin, have turned our cities to glorified dumpsites. The lignocellulosic agricultural wastes have no specific technical usage apart from the generation of fossil fuel. Maize tassel (MT), an agricultural waste, is the male flowering part of the maize plant. The tassel is the stemmy flower that sits on the apex of the maize stalk. These tassels, during pollination through cross-fertilization, are responsible for the production of kernel which in turn produces the maize cob. The whole process involved the tassel-producing pollen, which is blown off by wind in order to reach the silk ear (female flowering part of maize plant) for fertilization. MT has no production value after fertilization except for the farmer to cut them off in ensuring maximum utilization of maize grain production.

The possible use of MT as a biosorbent for inorganic compounds has been extensively explored by different researchers (Zvinowanda et al. 2008a, b, c), while its application in commercial production of activated carbon (AC) has not been fully explored. Apart from maize tassels, activated carbon has been produced from other diverse organic materials rich in carbon such as different agricultural wastes, coal, lignite, and wood (Daud and Ali 2004; Prahas et al. 2008; Olorundare et al. 2012). The possible use of agricultural residues in the production of good quality AC has been highlighted by a

number of researchers, mainly due to their availability, renewal ability, and low cost (Hu and Srinivasan 1999; Diao et al. 2002; Mozammel et al. 2002; Baquero et al. 2003; Sekar et al. 2004; Srinivasakannan and Bakar 2004; G´omez-Serrano et al. 2005; Puziy et al. 2005; Prahas et al. 2008).

Activated carbon can be defined as the final product of an activation process of carbonaceous materials from diverse sources and has over 60 % of carbon content (Bansal et al. 1988). It is composed of interconnected domains of benzene rings and graphite plate organized with some localized order on a molecular level (Bansal and Goyal 2005). It also has displaced extended interparticulate surface area and high degree of porosity (Bansal et al. 1988). The properties of the raw materials both in terms of physical and chemical compositions, as well as the process condition and method employed for activation, determined the adsorption properties of AC and its pore size distribution (Bota et al. 1997). AC can be produced in two ways: physical and chemical methods. These two methods employ a two-stage process in their operation, i.e. carbonization and activation. In the physical activation method, carbonization of precursors followed by activation with an oxidant such as steam, air, or $CO_2$ takes place. While in the chemical activation method, the two-step process occurs simultaneously with the impregnation of the precursor using dehydrating agents (such as acid or alkali) and oxidants. The reason for carbonization is to create initial porosity and ordering of the carbon structure and to enrich the carbon material, while the purpose of the activation process is to enhance the carbon structure by widening the pores, thereby making it more porous (Daud and Ali 2004). There are various parameters that affect the production of AC, its structure, or porosity. These parameters include (1) activating agents such as phosphoric acid, nitric acid, steam, carbon (IV) oxide, nitrogen, zinc chloride, hydrogen peroxide, potassium oxide, and sodium hydroxide; (2) activation temperature; (3) dynamic process in the films; (4) high density of the precursor; (5) low ash content of the precursor; and (6) high adsorption capacity. However, the activation process can only be ensured under certain condition, which is a non-limiting mass transfer condition which makes the reaction to occur at the particle's internal surface (Daud and Ali 2004; Prahas et al. 2008). For example, in chemical activation, the activation of the precursor takes place at a temperature lower than that of physical activation, and also, its yield is much higher than the physical one (Hu et al. 2001; Sudaryanto et al. 2006). Chemical activation also favours good porous structure (Ahmadpour and Do 1996), whilst the type of oxidant or dehydrating agents used is very crucial in porous development during the activation process, especially in lignocellulosic materials, which have not been carbonized. Among the dehydrating agents employed as activating agents, phosphoric acid is the most preferred oxidant. This is because of the environmental problems associated with the others such as zinc chloride that causes corrosion and inefficient chemical recovery (Srinivasakannan and Bakar 2004). The nature of porosity and the surface area have been reported to have a great influence in the processing or production of AC (Vernersson et al. 2001; Srinivasakannan and Bakar 2004; Sudaryanto et al. 2006; Prahas et al. 2008). Generally, dehydrating agents such as phosphoric acid can be grouped into two categories: one- and two-stage activation processes (impregnation and carbonization) carried out in either self-generated or inert-made atmosphere. Optimizing the process parameters such as the impregnation ratio, activating temperature, and activating time goes a long way to determine the nature of the produced AC. It has been reported that the ratio of the activating agents to the precursor is an important variable to porosity development in AC (Ahmadpour and Do 1997). Other operational variables like the method of mixing, activation temperature, and activation time do had a direct effect on porosity development (Ahmadpour and Do 1997; Guo and Rockstraw 2006).

To the best of our knowledge, there has been no report on the effect of impregnation ratios (IR) on AC produced from MT. In this study, phosphoric acid was used as the activating agent for the production of AC from MT, and the effect of the IR on the porosity and surface characterisation of the AC produced was investigated, as well as pore characterisation using various techniques.

## 2 Experimental Method

### 2.1 Reagents

Phosphoric acid and phenol used in the synthetic procedures of this work were of analytical grade and obtained from Sigma-Aldrich (St Louis, MO, USA). Distilled water was used for all synthesis and treatment processes.

## 2.2 Preparation of Activated Carbon

The precursor for the AC was acquired by collecting maize tassel (MT) 'grace green' cultivar variety from a local farm settlement near Vereeniging, 70 km away from the city of Johannesburg, South Africa. The dried woody parts of the maize plant were thoroughly washed and rinsed with deionised water and were thereafter oven-dried for 24 h at 110 °C. The tassels were then milled in a laboratory hammer mill (JANKE & KUNKEL micro-hammer mill) to obtain a fine powder. The resultant powder was fractionated into different sizes using analytical sieves. Particles of various diameters ranging from 45 to 212 μm were obtained, and the particle size 106 μm was used for the preparation of the AC. The dried reduced powdered of MT was then stored in a desiccator before use.

The chemical activation method using phosphoric acid was used to activate the precursor. The final sample preparation was done according to Olorundare et al. (2012) with little modification. Twenty grams of an aliquot of MT powder was added to 20 mL of phosphoric acid solution (85 % by weight) and manually stirred for 30 min and left to stand overnight. The physicochemical properties of the carbon-impregnated material (Xp) were investigated by varying the weight of the precursor to acid ratios, i.e. 1:1, 1:2, 1:3, 1:4 and 1:5, respectively. The produced AC were coded as ACC (i.e. ACC1, ACC2, ACC3, ACC4 and ACC5, respectively, based on their impregnation ratios), where ACC denotes chemical activation. The resulting slurry, the mixture of the precursor and phosphoric acid, then turned black yielding a black and sticky dry powder (depending on the ratio of impregnation). This was then semi-carbonized at the first stage before activation at the second stage (the black and sticky dry powder) at 500 °C in a horizontal tubular reactor furnace for an hour under inert atmosphere. Carbonization was performed under a nitrogen flow of 200 $cm^3$ $min^{-1}$ for 60 min. After activation, the AC produced was collected and cooled in a desiccator. The AC produced was then washed repeatedly with hot deionised water until constant pH of the solution was reached. The AC produced was then dried in a vacuum oven at 110 °C for 24 h, before being stored in a desiccator for later experimental use.

## 2.3 Characterisation of ACC

The pore structures of the resulting ACs were analysed using $N_2$ adsorption BET (Brunauer, Emmett and Teller) method for surface area, X-ray diffraction (XRD) for crystallinity, scanning electron microscopy (SEM) for morphological determination and Fourier transmission-infrared (FT-IR) for surface functional group.

### *2.3.1 $N_2$ Adsorption*

The characterisation of the pore structures of the resulting ACs was determined by nitrogen adsorption-desorption isotherm measured at 77 K using an ASAP 2020 Micromeritics instrument. Prior to gas adsorption measurements, the AC was degassed at 250 °C in a vacuum condition for a period of at least 5 h. Nitrogen adsorption isotherms were measured over a relative pressure ($P/P_o$) range from approximately 0.005 to 0.995. The BET surface area was determined by means of the standard BET equation applied in the relative pressure range from 0.05 to 0.3. The total pore volume was calculated at a relative pressure of approximately 0.995, and at this relative pressure, all pores were completely filled with nitrogen gas.

### *2.3.2 Scanning Electron Microscopy*

The SEM images were recorded for studying the surface morphology using a scanning electron microscope (SEM) (Nano 2000 High Resolution SEM (HRSEM), Jeol, Japan). Prior to applying the technique, the ACC was properly processed in order to obtain cross-sectional SEM micrographs. The ACC sample used was a finely processed powder which was added to the surface of the SEM sample holder already coated with carbon template which served as the base for the sample. The sample was then sprayed with sample spray coat in order for the entire grain particle to firmly attach to the sample and prevent cross-contamination of the sample in the sample holder compartment of the instrument. The samples were then transferred to the SEM specimen chamber and observed at an accelerating voltage of 5 kV, spot size of 8, aperture of 4, and working distance of 20 mm. Afterwards and during the segmentation stage, the micrograph section corresponding to the porous region of ACC was identified.

### *2.3.3 X-ray Diffraction*

The composition and structure of the samples were analysed by X-ray powder diffraction (XRD, SHIMADZU XRD 3000 diffractometer) at 40 kV and

40 mA and a scanning rate of 6°/min with 2$\theta$ ranging from 5° to 60° at a step size of 0.01°.

### 2.3.4 Fourier Transmission-Infrared Spectroscopy

The characterisation of the AC was performed by Fourier transform-infrared spectroscopy (FT-IR) to identify its surface functional groups. A quantitative analysis of the produced AC was conducted by obtaining FT-IR transmission spectra of the produced AC samples by the KBr technique using the ratio of 1:20. The technique involved placing dried KBr powder alone and later with the sample in an agate mortar and then ground into a fine powder before placing the mixture into the sample cup and later its surface was evened in a sample pressing bar to form a pellet. The two pellets, KBr and KBr sample mixture, were mounted one after the other onto the instrument to make a background measurement and sample measurement in the transmittance %T mode. FT-IR spectroscopy was then performed using a Perkin Elmer® Spectrum 100 FT-IR spectrometer, and the spectra were recorded with characteristic peaks in wave numbers from 450 to 4,000 $cm^{-1}$ at a resolution of 4 $cm^{-1}$ with 16 runs per scan. The elemental analysis of the produced AC was carried out using Perkin Elmer 2400 C, H, N, and O analyser.

## 2.4 Adsorption Studies

The isotherm adsorption studies were undertaken using simulated wastewater to assess the efficiency of the adsorbent for the removal of phenol from the aqueous solution using the batch method. The batch adsorption experiments were carried out in a 250-mL Erlenmeyer flask by shaking constant mass (0.04 g) of a predetermined size of adsorbent with constant volume (50 ml) of phenol solutions of increasing initial phenol concentrations (50–250 mg/L) to maintain constant mass to volume ratio. The pH of the solutions was adjusted accordingly by adding either 0.1 M HCl or 0.1 M NaOH. Each flask was sealed using rubber bung and kept in a state of agitation (150 rpm) using a mechanical laboratory shaker for the material to reach equilibrium. Upon equilibrium, the samples were filtered and analysed using UV-2450 UV/Vis spectrophotometer (Shimadzu, Japan). The first part of the filtrate was discarded to avoid the effects of phenol adsorption on the filter paper. All measurements of the ten scans were made at a wavelength corresponding to the maximum absorbance of 270 nm, the wavelength obtained after a full scan at the range of 200 to 600 nm. The amount of phenol adsorbed onto the AC was measured by subtracting the remaining concentrations of the phenol solution from the initial concentration. The effects of pH, contact time, and initial concentration of the adsorbent on the adsorption process were studied.

$$R(\%) = \frac{C_o - C_e}{C_o} \times 100 \quad (1)$$

The percentage removal ($R$) is denoted by Eq. (1) which determines the efficiency of the adsorbent. $C_o$ is the initial concentration and $C_e$ is the concentration at equilibrium.

The equilibrium adsorption capacities ($q_e$) of the AC at pre-determined time intervals were determined based on adsorbate mass balance using Eq.(2):

$$q_e = \left(\frac{C_o - C_e}{M}\right) V \quad (2)$$

where $C_o$ and $C_e$ are the initial and equilibrium concentrations of phenol (milligram per liter), respectively; $V$ is the volume of the aqueous solution (liter); and $M$ is the mass of activated carbon used (gram).

$$q_t = \left(\frac{C_o - C_t}{M}\right) V \quad (3)$$

The equilibrium adsorption ($q_t$) at time $t$ is the concentration of phenol adsorbed at time $t$ and is given by Eq. (3). $C_o$ and $C_e$ are the initial and equilibrium concentrations at time $t$, $V$ is the volume of the aqueous solution (liter) and $M$ is the mass of activated carbon used (gram).

## 2.5 Isotherm Modeling

The equilibrium experimental data between the concentration of the phenol adsorbed from the solution ($C_e$) and the amount of phenol adsorbed ($q_e$) onto ACC at constant temperature and pH were described by the optimum adsorption isotherm model. The linear forms of the isotherm model of Langmuir and Freundlich equations were used to describe the equilibrium experimental data, using the correlation coefficients ($R^2$) to compare these equations (Ho and McKay 1999; Ho and Ofomaja 2006; Srivastava et al. 2006; Gaspard et al. 2007; Hameed and Rahman 2008; Jaramillo et al. 2010; Elmorsi 2011).

### 2.5.1 Langmuir Isotherm

The Langmuir isotherm is a mechanistic model that is used to predict the adsorption of aqueous compounds onto solid phase (Ho and McKay 1999; Ho and Ofomaja 2006; Hameed and Rahman 2008; Elmorsi 2011). The model assumes that adsorption is done over a uniform adsorbent surface at a constant temperature by a monolayer of adsorbed material (in a liquid, such as phenol) and that the equilibrium constant controlled the distribution of the compound between the two phases. Thus, at equilibrium, both the adsorption and desorption rates are equal, as described by Lineweaver-Burk (Langmuir-I) (Ho and McKay 1999; Ho and Ofomaja 2006; Hameed and Rahman 2008; Elmorsi 2011). Thus, Langmuir-I equation is given as:

$$q_e = \frac{q_m K_L C_e}{1 + K_L C_e} \tag{4}$$

where $q_m$ (the maximum capacity of adsorption, milligram per gram) and $K_L$ (constant related to the affinity of the binding sites, liter per milligram) are the Langmuir isotherm constants.

### 2.5.2 Freundlich Isotherm

The Freundlich isotherm model describes the adsorption process that takes place on a heterogeneous surface (Ho and McKay 1999; Ho and Ofomaja 2006; Hameed and Rahman 2008; Elmorsi 2011). Thus, the Freundlich exponential equation is given as:

$$q_e = K_F C^{1/n} \tag{5}$$

where $K_F$ (liter per milligram) is the indicator of the adsorption capacity and $\frac{1}{n}$ is the adsorption intensity which indicates the heterogeneity of the adsorbent sites and the relative distribution of energy. The linear form of this model is derived by taking the logarithm of the term in Eq. (5) as shown in Table 1.

## 3 Results and Discussion

Parameters such as impregnation ratio, concentration of oxidant, activation time, and activation temperature could impact significantly on the characteristics of the porous structure of the AC produced. The above parameters have been reported by other workers to impart significantly on the characteristic of the surface chemistry and porosity of AC (Diao et al. 2002; Srinivasakannan and Bakar 2004; G´omez-Serrano et al. 2005; Puziy et al. 2005). Impregnation ratio and the pre-carbonization process were investigated in this study. All the experimental data were repeated thrice with relative standard deviation less than 10 %. Furthermore, the AC produced were also characterised using FT-IR, SEM, $N_2$ adsorption and XRD.

### 3.1 Effects of Impregnation Ratio on Elemental Analysis and Pore Structure of the Produced AC

The effect of impregnation ratio (IR) on the elemental composition and pore volume is discussed. The results obtained in this study (Table 2) show that the precursor (MT) has a high percentage of fixed carbon, an indication of its applicability in AC production. However, the specific surface area ($S_{BET}$) and the total pore volume ($V_{Total}$) of the AC at different IR were also investigated. From the results of elemental analysis, it was observed that the contents of elements were almost the same for the different IR, except for the value of nitrogen where all the elemental nitrogen was reduced to nitrogen gas. But the values of the specific surface area ($S_{BET}$) and the total pore volume ($V_{Total}$) of the produced AC prepared with different IR were obviously different (Table 3). The results showed that $S_{BET}$ and $V_{Total}$ increased with increase in IR, reaching maximum for $S_{BET}$ at 1,263 $m^2/g$ and 1.59 $cm^3/g$ for $V_{Total}$ when the IR was 1:4 and 1:5, respectively. The reason was that with the increase in IR, the acid was able to penetrate the interior of the particle of the produced AC to a certain extent until no further

**Table 1** Different linear and non-linear isotherm models used in this study

| Isotherm | Non-linear form | Linear form | Plot |
|---|---|---|---|
| Langmuir-I | $q_e = \frac{K_L C_e}{1 + K_L C_e}$ | $\frac{1}{q_e} = \left(\frac{1}{K_L q_m}\right)\frac{1}{C_e} + \left(\frac{1}{q_m}\right)$ | $\frac{1}{q_e}$ vs. $\frac{1}{C_e}$ |
| Freundlich | $q_e = K_F C_e^{1/n}$ | $\log q_e = \log K_F + \frac{1}{n} \log C_e$ | $\log q_e$ vs. $\log C_e$ |

**Table 2** Elemental analysis of maize tassel and produced activated carbon

| Sample code | C | H | H/C | N | S | O[a] | % Yield |
|---|---|---|---|---|---|---|---|
| Maize tassel | 53.25 | 5.63 | 0.11 | 1.15 | 0.081 | 39.88 | – |
| IR(1:1) ACCT500 | 41.65 | 1.37 | 0.033 | 0 | 0 | 56.37 | 56.96 |
| IR(1:2) ACCT500 | 56.17 | 1.66 | 0.030 | 0 | 0 | 42.18 | 46.67 |
| IR(1:3) ACCT500 | 56.43 | 1.99 | 0.035 | 0 | 0 | 41.55 | 42.36 |
| IR(1:4) ACCT500 | 51.51 | 1.47 | 0.029 | 0.034 | 1.090 | 45.93 | 39.50 |
| IR(1:5) ACCT500 | 50.45 | 1.38 | 0.029 | 0 | 1.040 | 47.13 | 38.40 |

*IR* impregnation ratio, *ACC* chemical activated carbon, *H/C* hydrogen carbon ratio

[a] Obtained by difference

reaction could take place. This result is similar to those obtained by Prahas et al. (2008) and Wang et al. (2011).

### 3.2 Effect of Impregnation Ratio on Yield of the Produced Activated Carbon

Figure 1 shows the effect of IR on the yield of AC produced, which is usually defined as the final weight of AC after activation, washing, and drying divided by the initial weight of the precursor on a dry mass basis (Diao et al. 2002). The results obtained show that the yield of AC produced from MT at different IR decreases with increasing IR. In this study, the values obtained ranged from 38.40 to 56.96 %. This is similar to what has been reported by other workers such as Guo and Rockstraw (2006) who used cellulose and obtained 42–51 %, Puziy et al. (2005) who used fruit stones and obtained 31.9–48.5 %, Srinivasakannan and Bakar (2004) who used rubber wood sawdust and obtained 46.63 % and G´omez-Serrano et al. (2005) who used chestnut wood and obtained 37.2–42.3 %. The yield obtained for the phosphoric acid-activated MT was higher than those obtained for fixed carbon in the precursor (Table 2). This is because carbonization at high temperature affects the polymeric structures which easily decompose to liberate gaseous substances from the lignocellulosic material in the form of liquid/or tar before forming a rigid carbon skeleton in the form of an aromatic sheet (Rodriguez-Reinoso and Molina-Sabio 1992; Teng et al. 1998).

Figure 1 also revealed that the carbon yield decreased with an increase in IR from 1 to 5. It has been reported (Jagtoyen and Derbyshire 1998; Timur et al. 2006) that during lignocellulosic reaction with phosphoric acid, the first acid attack occurs immediately after the mixing of lignin and hemicelluloses. This can be explained by the fact that cellulose is more resistant to acid hydrolysis (Jagtoyen and Derbyshire 1998). This reaction is followed by a series of other reactions, namely, dehydration, degradation and condensation. IR, which occurs through excess phosphoric acid, promotes gasification of char, thereby increasing the total weight loss of carbon (Jagtoyen and Derbyshire 1998; Teng et al. 1998; Timur et al. 2006; Prahas et al. 2008.

### 3.3 Effect of Impregnation Ratio on the Surface Area and Pore Volume of the Produced Activated Carbon

The effects of impregnation ratio on the BET surface area, micropore volume and total pore volume are given in Table 3. The total pore volume, $V_{Total}$, was calculated from nitrogen adsorption data as the volume of liquid

**Table 3** Pore structure of produced activated carbon

| Sample code | $S_{BET}$ ($m^2/g$) | $S_{Langmuir}$ ($m^2/g$) | $S_{singlepoint}$ ($m^2/g$) | $V_{Total}$ ($cm^3/g$) | $V_{micro}$ ($cm^3/g$) | $V_{meso}$ ($cm^3/g$) |
|---|---|---|---|---|---|---|
| IR(1:1) ACCT500 | 712 | 967 | 698 | 0.373 | 0.0803 | 0.292 |
| IR(1:2) ACCT500 | 776 | 1,068 | 748 | 0.623 | 0.0141 | 0.609 |
| IR(1:3) ACCT500 | 623 | 850 | 600 | 0.617 | 0.0197 | 0.597 |
| IR(1:4) ACCT500 | 1,263 | 1,735 | 1,214 | 1.541 | 0.0327 | 1.508 |
| IR(1:5) ACCT500 | 1,240 | 1,713 | 1,182 | 1.592 | 0.0262 | 1.566 |

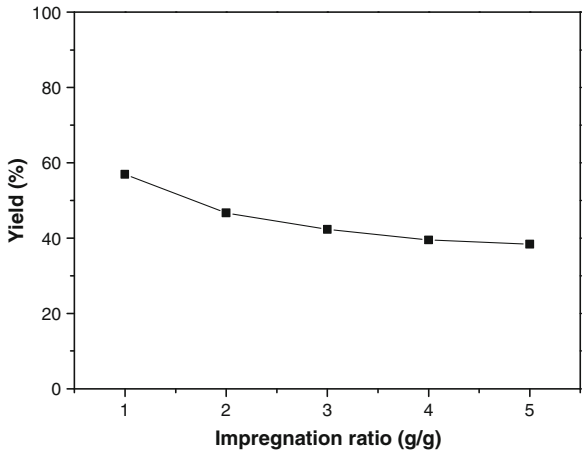


**Fig. 1** Effect of impregnation ratio on the produced activated carbon

nitrogen at a relative pressure of 0.995. The micropore volume, $V_{micro}$, was determined by the DFT method, and the mesopore volume, $V_{meso}$, was obtained by subtraction of the micropore volume and the total pore volume, $V_{Total}$.

The specific surface area ($S_{BET}$) and the total pore volume ($V_{Total}$) increase with the increase in IR. The increase in porosity with temperature greater than 450 °C can be attributed to the formation of tars, which is caused by the acid treatment on the lignocellulosic material (Hsu and Teng 2000). At temperatures greater than 450 °C (i.e., 500 °C activation temperature for this study), an increase in IR also increased the micropore volume, but an increase of micropore volume at IR(1:2) ACCT500 and IR(1:3) ACCT500 was not significant (Figs. 2 and 3). On the other hand, the mesopore volumes increased with the increase in IR. Furthermore, phosphoric acid-produced mesopore has been reported by some workers (Laine et al. 1989; Teng et al. 1998; Timur et al. 2006). Moreover, it was observed that IR(1:3) ACCT500 produced a pore structure with a low specific surface and micropore and mesopore volume. This might have resulted from contraction of carbon structures which in turn resulted in low porosity of the pore structure of AC. Similar results have been reported by other workers (Prahas et al. 2008).

### 3.4 Effect of Impregnation Ratio on $N_2$ Adsorption-Desorption Isotherms of Porous Carbons

Figure 4 shows the effect of $N_2$ adsorption-desorption isotherms of the AC prepared under different IR at 500 °C for 60 min. In the isotherm classification according to BET (Bansal and Goyal 2005; Namane et al. 2005), in this study, IR(1:1) ACCT500 belongs to type I (1:1), IR(1:2) ACCT500 to type II (1:2), IR(1:4) ACCT500 to type III (1:4) and IR(1:3) ACCT500 and IR(1:5) ACCT500 to type IV (1:3 and 1:5). For the samples IR(1:1) ACCT500 and IR(1:2) ACCT500, the adsorption of $N_2$ increases rapidly at lower relative pressure which indicates that the AC produced had a well-developed mesopore in its matrix. While in the case of samples IR(1:4) ACCT500 and IR(1:5) ACCT500, the volume of $N_2$ adsorbed was found to increase with the increase in IR at higher relative pressure greater than 0.05. The hysteresis loop for the samples occurred at around 0.45 relative pressure. The volume of the adsorbed $N_2$ was different in all cases for the samples,

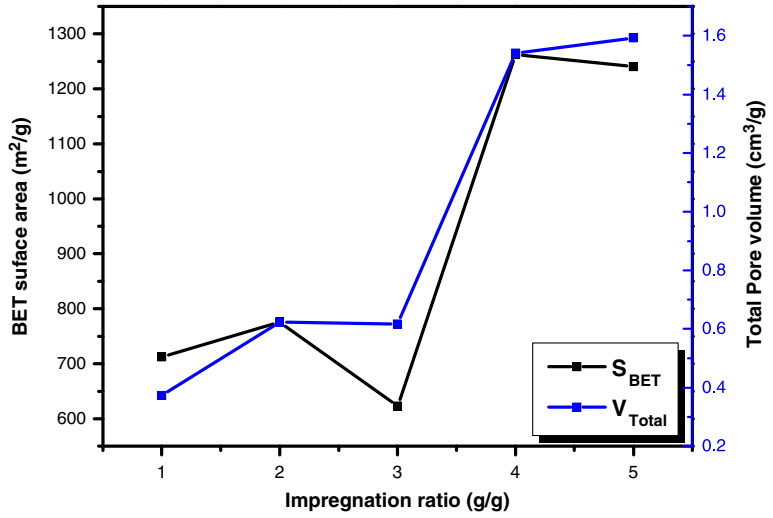


**Fig. 2** Effect of impregnation ratio on specific surface area and total pore volume of the produced AC

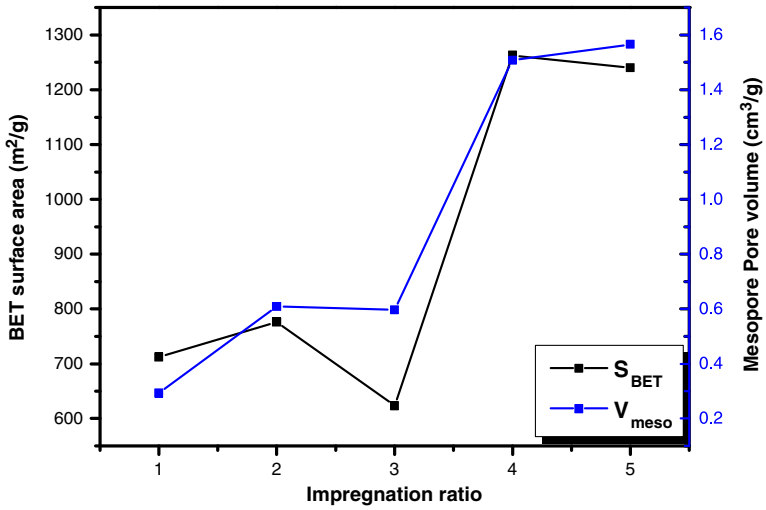


**Fig. 3** Effect of impregnation ratio on specific surface area and mesopore volume of the produced AC

indicating that changes in the value of IR have a significant impact on the porosity of the AC.

### 3.5 Effect of Impregnation Ratio on the Crystallinity of the Produced Activated Carbon

Figure 5 shows the effect of X-ray diffraction patterns of the produced AC prepared under different IR at an activation temperature of 500 °C for 60 min. The figure shows two broad peaks at 26° and 43°, and these are assigned to reflection from the plane (0 0 2) and the overlapped reflections from 1 0 0 and 1 0 1 planes, respectively. The appearance of these peaks in the produced AC indicates increasing of crystalline structure with increasing IR, which results in better layer alignment. The pattern shows a broad diffraction peak in $2\theta$ range of 10–30°. The XRD pattern obtained in this study is similar to what has been reported previously by other workers (Ruland and Smarsly 2002; Lua and Yang 2004; Prahas et al. 2008; Wang et al. 2009, 2011).

### 3.6 Scanning Electron Microscopy Analysis

The scanning electron micrograph result of the surface morphology of the produced AC, which described the surface composition of AC, is illustrated in Fig. 6. The result shows that IR has a significant impact on AC porosity. This is obvious in the differences of the exterior surfaces of the AC produced. In samples IR(1:2) ACCT500, IR(1:3) ACCT500, IR(1:4) ACCT500 and IR(1:5) ACCT500, there are pronounced cavities on the exterior surfaces which might have resulted from the evaporation of the phosphoric acid during the carboni-

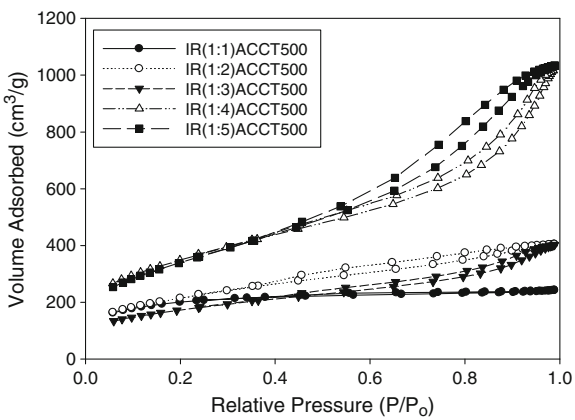


**Fig. 4** Effect of impregnation ratio on $N_2$ adsorption of the activated carbon

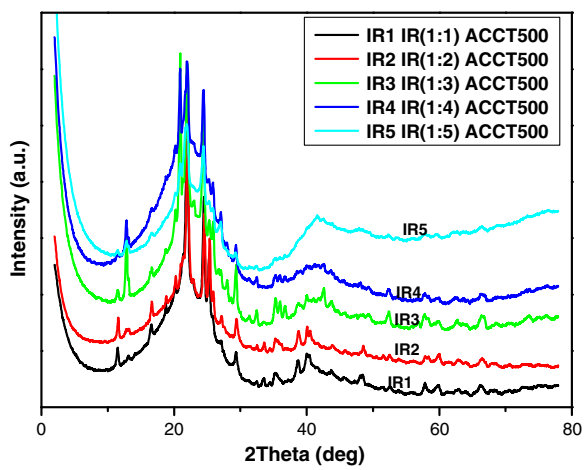


**Fig. 5** XRD of the produced activated carbon at different impregnation ratios

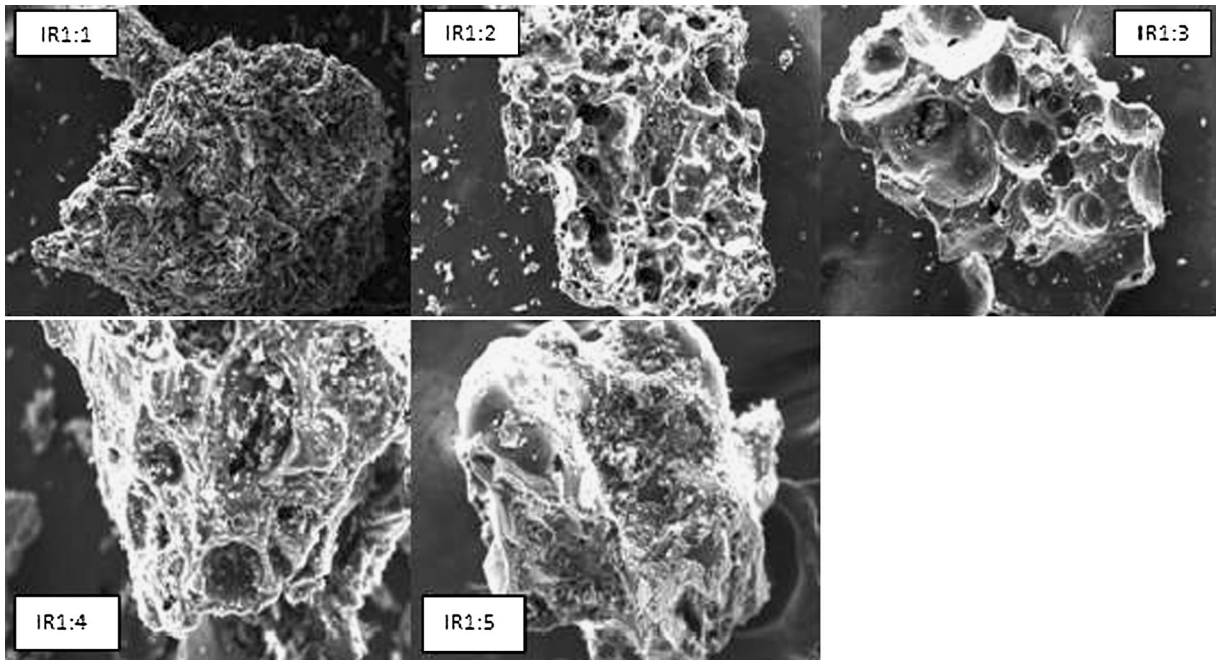


**Fig. 6** SEM micrograph of the produced activated carbon at different impregnation ratios

zation, thereby leaving spaces previously occupied by the dehydrating agent. In Fig. 6, IR(1:4) ACCT500 revealed that the surface of the produced AC was quite dense with both large and small pores and spongy white patches with occasional crack in the carbon matrix. This accounts for its large surface area, while in the case of IR(1:3) ACCT500, the surface reveals smooth collapsed surfaces having a depression with some block pores which explain its low surface area and pore volume. However, as the ratio of impregnation increases with adequate mixing, the surface area increases as shown in IR(1:4) ACCT500, but decreases in IR(1:5) ACCT500. This might be due to evaporation of the dehydrating agent previously occupying the cavities or excess activating agents that are still filling the pores of the porous carbon.

### 3.7 Fourier Transform-Infrared Analysis

The effect of various IR at the activation temperature of about 500 °C on surface functional group is shown by the FT-IR spectra in Fig. 7. Figure 7 shows the FT-IR spectra of the produced AC with various IR at the activation temperature of about 500 °C. All the samples show broadband absorption spectra around 3,400–2,850 $cm^{-1}$. A peak around 1,760–1,640 $cm^{-1}$ shows the presence of C=O stretching vibration of aldehyde, carboxylic acid, ketones and esters. The presence of a broadband around 3,400–2,850 $cm^{-1}$ and peak around 1,670 $cm^{-1}$ indicates the presence of carboxylic acid (Boonamnuavitaya et al. 2003; Guo and Rockstraw 2006). A broad peak of relatively low intensity at an absorption band of 3,300–3,100 $cm^{-1}$ of the broadband around 3,400–2,850 $cm^{-1}$ may be assigned O–H stretching vibration in phenol and C–H stretching in alkane. The weak peak around 2,850 $cm^{-1}$ is C–H stretching vibration in the methyl group (Boonamnuavitaya et al. 2003). A strong band at 1,646 $cm^{-1}$ can be assigned to C=C aromatic ring stretching vibration, which is enhanced by polar functional and alkene groups (Puziy et al. 2005). Furthermore, there is a sharp peak at 1,410 $cm^{-1}$, which corresponds to C–H stretching alkane, and also a broadband between 1,300 and 1,000 $cm^{-1}$ with the strong band around 1,220 $cm^{-1}$ and a shoulder around 1,100 $cm^{-1}$ (which occurred in all the samples with various intensities). Puziy et al. (2005) reported similar peaks at 1,220–1,180 $cm^{-1}$, which were assigned to the O=C stretching vibrations in P–O–C, the stretching mode of hydrogen-bonded P=O and P=OOH linkage. The shoulder at 1,203–1,118 $cm^{-1}$ can be assigned to a symmetrical vibration in a chain of P–O–P and ionised linkage $P^{+}$–

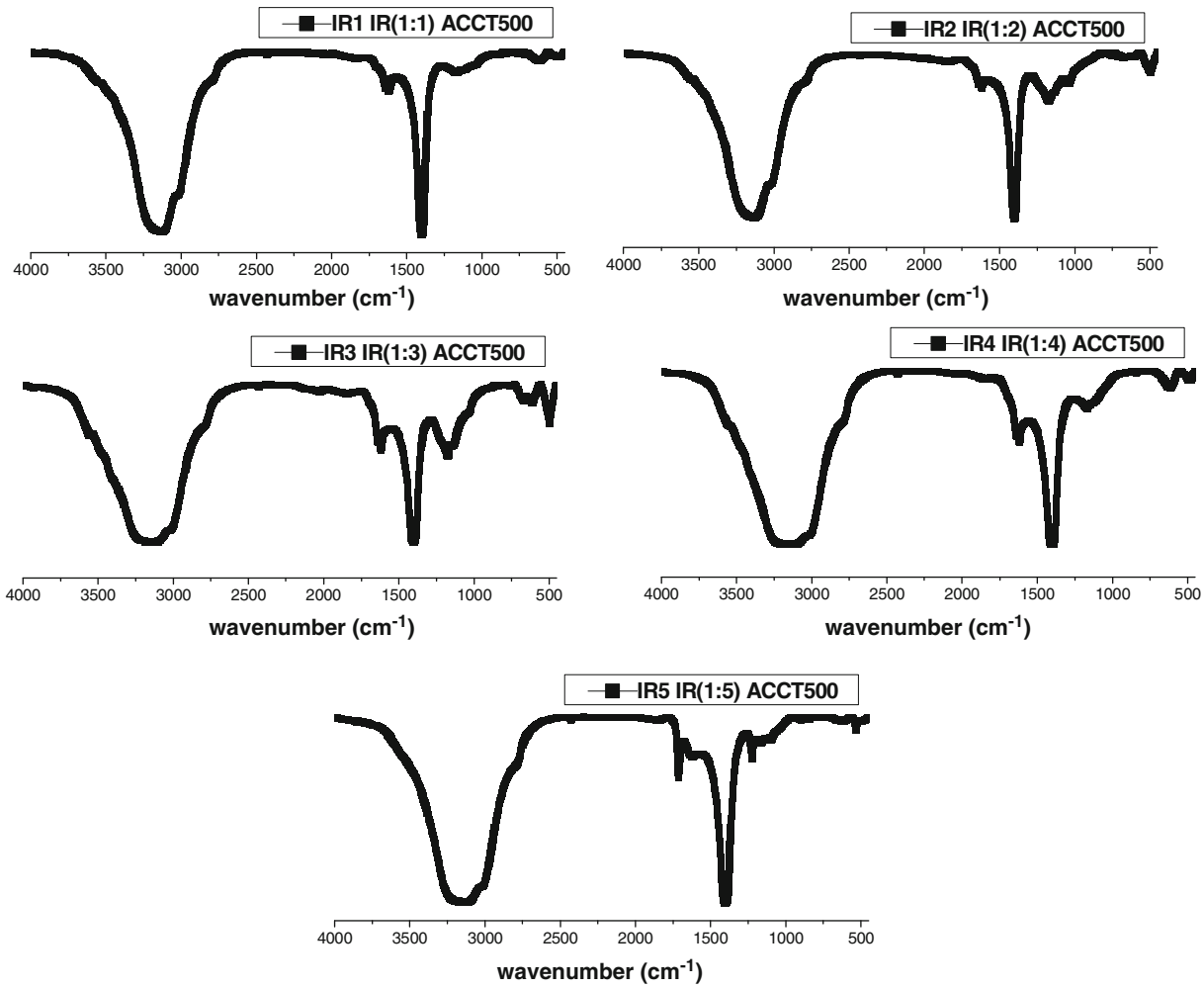


**Fig. 7** FT-IR spectra of the produced activated carbon at different impregnation ratios

$O^-$ in acid phosphate esters. The phosphorous-containing group becomes more obvious as the IR increases with the help of the activation temperature.

### 3.8 Pore Size Distribution

Pore size distribution in the produced AC characterises the structural heterogeneity of a porous material, which also represents a model of solid internal structure (Bansal and Goyal 2005; Demiral et al. 2011). Sudaryanto et al. (2006) reported that pore size distributions are closely related to both equilibrium and kinetic properties of a porous material. However, according to the International Union of Pure and Applied Chemistry (IUPAC), structural characterisations in terms of pore size are classified into three groups, namely, micropore (diameter <2 nm), mesopore (diameter between 2 and 50 nm) and macropore (diameter >50 nm) (Demiral et al. 2011; Namane et al. 2005). In all the results obtained, the pore size distribution falls between the micropore and mesopore (Table 3 and Fig. 8). Figure 8 reveals the pore size distribution of the produced AC. From Fig. 8, in IR(1:1–1:4) ACCT500, it could be deduced that a major peak lies in the mesopore region for all the samples, while the other minor peak is in the micropore region which is not visible. The mesopore volume is larger than the micropore volume (Table 3). The ratio of $V_{meso}$ to $V_{Total}$ ranges from 0.783 to 0.983. As IR increases, the mesoporosity of the produced AC increases because the dehydrating agent reacts first with

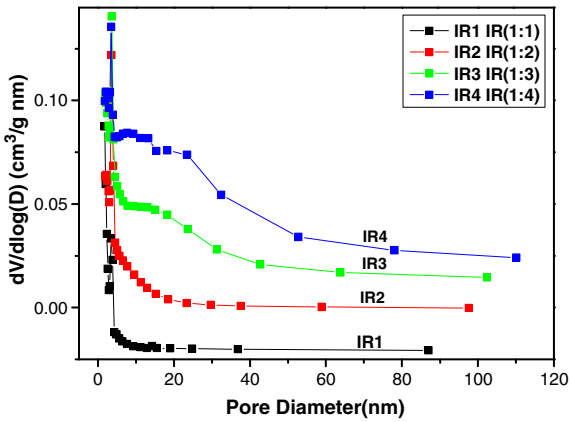


**Fig. 8** Pore size distribution of the produced activated carbon

lignin and hemicelluloses to create the mesopore structure. Similar results have been reported by other workers (Prahas et al. 2008; Wang et al. 2011).

### 3.9 Effect of Contact Time and Initial Concentration on Phenol Adsorption

Figure 9 shows the effect of contact time on the removal of phenol at various initial concentrations (50–250 mg/L) at 30 °C and optimum pH of 6. The saturation curve rises sharply at the initial stages, indicating that plenty of sites were readily accessible. After sometime, there were decreases in adsorption which led to a slight plateau, which indicates that the adsorbent has reached saturation point at this stage. However, in Fig. 10, there was a formation of a plateau indicating the saturation point of the adsorbent. It can also be seen from Fig. 10 that the contact time needed for phenol solutions with initial concentrations of 50–150 mg/L to reach equilibrium was 120 min. However, for phenol solutions with higher initial concentrations, longer equilibrium times were required which indicate a decrease in adsorption capacity (Fig. 9). It was also seen that an increase in initial phenol concentration resulted in increased phenol uptake. The removal curve in Fig. 10 is single and continuous, indicating the formation of monolayer coverage of the phenol molecules onto the outer surface of the adsorbent. A similar observation was reported by Moreno-Castillo et al. (1995) about the adsorption behaviour of mono-substituted phenols of different solubilities on activated carbons produced from both demineralised and original bituminous coal.

The removal percentage efficiency was over 90 % (Fig. 10). The adsorption capacity at equilibrium ($q_e$) increased from 12.51 to 75.29 mg/g with an increase in the initial phenol concentrations from 50 to 250 mg/L. The mass transport steps are determined by the adsorption of solute from the solution by the porous adsorbent (Gaspard et al. 2007). This occurs by the adsorbate migrating through the solution by film diffusion, which is then followed by solute movement from the particle surface into the interior site by pore diffusion, and then the adsorbate is absorbed into the active sites at the interior of the adsorbent particle (Gaspard et al. 2007; Hameed and Rahman 2008). The relative affinity between the carbon surface and phenolic molecules has been reported to be related to the complexes formed between the organic ring of the phenol and the basic sites on the carbon surface (Moreno-Castillo et al. 1995).

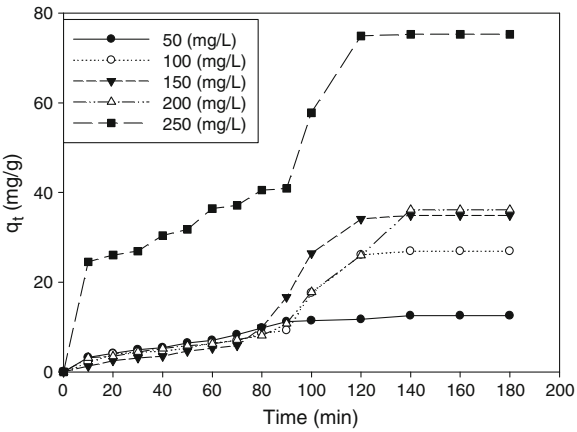


**Fig. 9** Effect of initial concentration and contact time on adsorption of phenol onto ACC

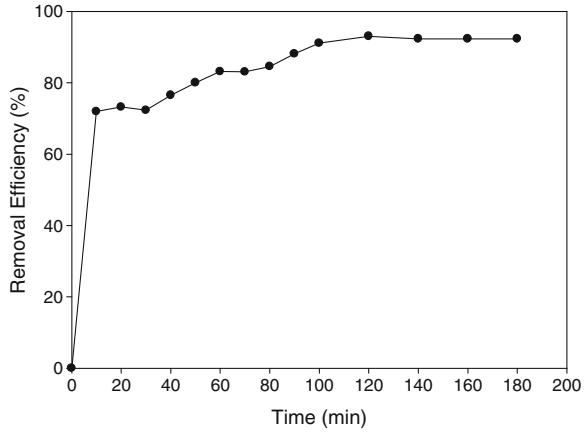


**Fig. 10** Effect of initial concentration and contact time on adsorption capacity of ACC

### 3.10 Effect of pH on Adsorption Properties of Activated Carbon

The influence of pH on the adsorptive capacity of the chemically produced AC was studied at room temperature (30 °C) using the initial concentration of 50 mg/L using solution pH values from 2 to 12. Figure 11 demonstrates that phenol adsorption was unaffected when the pH was low in the range of 2 to 4 and later showed an increase at pH greater than 4 and maximum at pH 6. A similar trend of the effect was reported by other workers using commercial and laboratory-produced activated carbon (Jankowska et al. 1991; Srivastava et al. 2006; Jaramillo et al. 2010). The pH solution affects the surface charge of the adsorbent and the degree of ionisation of the adsorbate (Aksu and Yener 2001; Hameed and Rahman 2008). Phenol as a weak acid compound (p*K*a≈9.89) often dissociates at pH>p*K*a (Moreno-Castillo 2004; Hameed and Rahman 2008). The adsorption decrease at high pH values is attributed to ionisation of the adsorbate molecules and electrostatic repulsions between the negative surface charge and the phenolate-phenolate anion in the solution (Moreno-Castillo 2004; Hameed and Rahman 2008).

### 3.11 Adsorption Isotherms

Basically, the adsorption isotherm is an important tool used to describe the way solutes interact with adsorbents and is also applicable in optimizing the use of adsorbent in adsorption studies. Experimental data obtained for the adsorbed phenol against initial concentration was analysed using different types of isotherms which include Langmuir and Freundlich equations (Jaramillo et al. 2010).

Langmuir and Freundlich isotherm models were used to describe the relationship between the amount of phenol adsorbed and its equilibrium concentration in solution. The isotherm that best describes monolayer adsorption on a finite number of identical sites is the Langmuir. The model does not consider transmigration in the plane of the surface, but assumes uniform adsorption on the surface (Parra et al. 1995; Srivastava et al. 2006). The linear form of the isotherm can be denoted by the following equation:

$$\frac{1}{q_e} = \left(\frac{1}{K_L q_m}\right)\frac{1}{C_e} + \left(\frac{1}{q_m}\right) \tag{6}$$

where $C_e$ (milligram per gram) is the equilibrium concentration, i.e. phenol ion concentration remaining in the solution at equilibrium; $q_e$ is the phenol ion concentration taken up by the sorbent per unit mass of the sorbent at equilibrium; and $q_m$ (the maximum capacity of adsorption, milligram per gram) and $K_L$ (constant related to affinity of the binding sites, liter per milligram) are the Langmuir isotherm constants. The plot of $\frac{1}{q_e}$ vs. $\frac{1}{C_e}$ gives a linear plot indicating that the sorption obeys the Langmuir model (Eq. 6). Figure 12 shows a linear plot of $\frac{1}{q_e}$ vs. $\frac{1}{C_e}$ using the experimental data obtained, suggesting the applicability of the of Langmuir model which results in $R^2$=0.95 and adsorption capacity of $q_m$=344.8 mg/g.

The Freundlich isotherm model describes the adsorption process that takes place on a heterogeneous surface

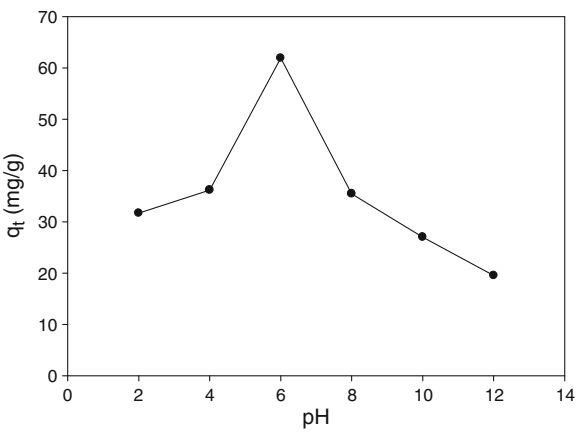


**Fig. 11** Effect of pH on adsorption properties of ACC

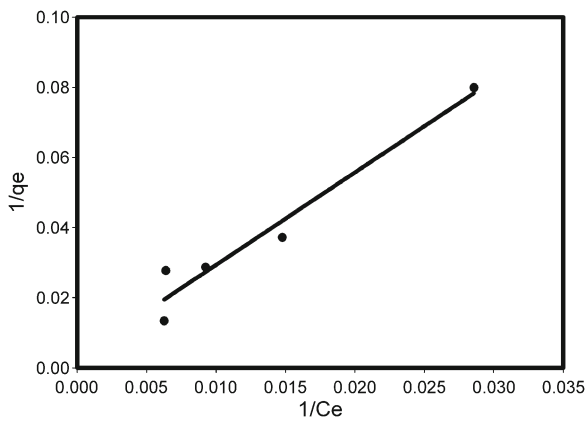


**Fig. 12** Langmuir isotherm adsorption of phenol onto ACC at 30 °C

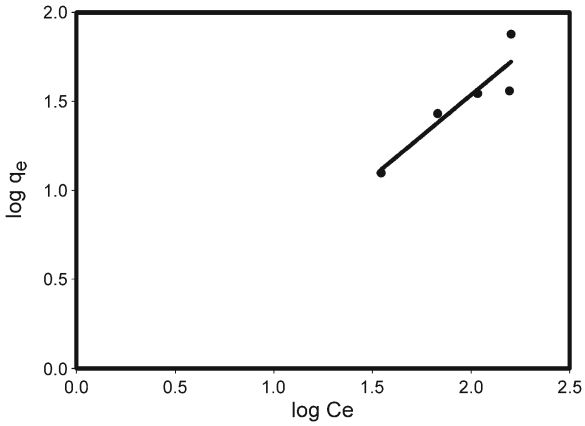


**Fig. 13** Freundlich isotherm adsorption onto ACC at 30 °C

(Ho and McKay 1999; Ho and Ofomaja 2006; Srivastava et al. 2006). Thus, the Freundlich exponential equation is given as:

$$q_e = K_F C^{1/n} \tag{7}$$

where $K_F$ (liter per milligram) is the indicator of the adsorption capacity and $\frac{1}{n}$ is the adsorption intensity which indicates the heterogeneity of the adsorbent sites and the relative distribution of energy. The linear form of this model is derived by taking the logarithm of the term in Eq. (7).

$$\log q_e = \log K_F + \frac{1}{n}\log C_e \tag{8}$$

The plot of log $q_e$ vs. log $C_e$ from Eq. (8) gives a linear plot with $\frac{1}{n}$ as the slope and ($K_F$=2.51 L/mg) as the intercepts (Fig. 13). The value of $\frac{1}{n}$ is 0.738, which is nearer to unity, suggesting the favourability of the Freundlich isotherm for the adsorption process.

## 4 Conclusion

The porous activated carbon AC was prepared from maize tassel (MT) using phosphoric acid as an activating agent. The effect of the impregnation ratio (IR) on the pore structure and surface chemistry was studied. The pore structure of the porous carbon produced was investigated by XRD, $N_2$ adsorption, FT-IR and SEM. The results obtained showed that IR has a direct relationship with pore structure. The activated carbon AC produced were porous having a maximum surface area of 1,263 $m^2$/g and total pore volume of 1.592 $cm^3$/g. Also, increasing IR also increases the acid functional group.

**Acknowledgments** The authors would like to acknowledge the University of Johannesburg for funding this research project.

## References

Ahmadpour, A., & Do, D. D. (1996). The preparation of active carbons from coal by chemical and physical activation. *Carbon, 34*, 471–479.

Ahmadpour, A., & Do, D. D. (1997). The preparation of activated carbon from macadamia nutshell by chemical activation. *Carbon, 35*, 1723–1732.

Aksu, Z. J., & Yener, A. (2001). Comparative adsorption/biosorption study of monochlorinated phenols onto various sorbents. *Waste Manag, 21*, 695–702.

Bansal, R. C., & Goyal, M. (2005). *Activated carbon adsorption*. Boca Raton: Taylor and Francis.

Bansal, R. C., Donnet, J. B., & Stoeekli, H. F. (1988). *Active carbon*. New York: Marcel Dekker.

Baquero, M. C., Giraldo, L., Moreno, J. C., Sua´rez-Garcı´a, F., Martı´nez-Alons, A., & Tasco´n, J. M. D. (2003). Activated carbons by pyrolysis of coffee bean husks in presence of phosphoric acid. *Journal of Analytical Applied Pyrolysis, 70*(2), 779–784.

Boonamnuavitaya, V., Sae-ung, S., & Tanthapanichakoon, W. (2003). Preparation of activated carbons from coffee residue for the adsorption of formaldehyde. *Separation Purification Technology, 42*, 159–168.

Bota, A., Laszlo, K., Nagy, L. G., & Schlimper, H. (1997). Active carbon from apricot pits. *Magyar Kemiac Folyoirat, 103*(9), 470–479.

Daud, W. M. A., & Ali, W. S. W. (2004). Comparison on pore development of activated carbon produced from palm shell and coconut shell. *Bioresour Technol, 93*, 63–69.

Demiral, H., Demiral, L., Karabacakoglu, B., & Tumsek, F. (2011). Production of activated carbon from olive bagasse by physical activation chem. *Engineering Research Design, 89*, 206–213.

Diao, Y., Walawender, W. P., & Fan, L. T. (2002). Activated carbons prepared from phosphoric acid activation of grain sorghum. *Bioresour Technol, 81*, 45–52.

Elmorsi, T. M. (2011). Equilibrium isotherms and kinetic studies of removal of methylene blue dye by adsorption onto miswak leaves as a natural adsorbent. *Journal of Environmental Protection, 2*, 817–827.

G'omez-Serrano, V., Cuerda-Correa, E. M., Fern´andez-Gonz´ales, M. C., Alexandre-Franco, M. F., & Mac´ıas-Garc´ıa, A. (2005). Preparation of activated carbons from chestnut wood by phosphoric acid-chemical activation. Study of microporosity and fractal dimension. *Material Letters, 59*, 846–853.

Gaspard, S., Altenor, S., Dawson, E. A., Barnes, P. A., & Quensanga, A. (2007). Activated carbon from vetiver roots: gas and liquid adsorption studies. *Journal Hazardous Material, 144*, 73–81.

Guo, Y., & Rockstraw, D. A. (2006). Physical and chemical properties of carbons synthesized from xylan, cellulose, and Kraft lignin by $H_3PO_4$ activation. *Carbon, 44*, 1464–1475.

Hameed, B. H., & Rahman, A. A. (2008). Removal of phenol from aqueous solutions by adsorption onto activated carbon prepared from biomass material. *Journal Hazardous Material, 160*, 576–581.

Ho, Y. S., & McKay, G. (1999). Pseudo-second order model for sorption processes. *Process Biochemistry, 34*(5), 451–465.

Ho, Y. S., & Ofomaja, A. E. (2006). Pseudo-second-order model for lead ion sorption from aqueous solutions onto palm kernel fiber. *Journal of hazardous materials, 129*(1–3), 137–142.

Hsu, L. Y., & Teng, H. (2000). Influence of different chemical reagents on the preparation of activated carbons from bituminous coal. *Fuel Process Technology, 64*, 155–166.

Hu, Z., & Srinivasan, M. P. (1999). Preparation of high-surface-area activated carbons from coconut shell. *Microporous Mesoporous Material, 27*, 11–18.

Hu, Z., Srinivasan, M. P., & Ni, Y. (2001). Novel activation process for preparing highly microporous and mesoporous activated carbons. *Carbon, 39*, 877–886.

Jagtoyen, M., & Derbyshire, F. (1998). Activated carbons from yellow poplar and white oak by $H_3PO_4$ activation. *Carbon, 36*, 1085–1097.

Jankowska, H., Swiatkowski, A., Choma, J. (1991). Active Carbon. Chichester, West Sussex: Ellis Horwood publisher.

Jaramillo, J., Modesto Alvarez, P., Gómez-Serrano, V. (2010). Oxidation of activated carbon by dry and wet methods surface chemistry and textural modifications. *Fuel Processing Technology, 91*(11), 1768–1775.

Laine, J., Calafat, A., & Labady, M. (1989). Preparation and characterization of activated carbons from coconut shell impregnated with phosphoric acid. *Carbon, 27*, 191–195.

Lua, A. C., & Yang, T. (2004). Effect of activation temperature on the textural and chemical properties of potassium hydroxide activated carbon prepared from pistachio-nut shell. *Journal of Colloid Interface Science, 274*, 594–601.

Moreno-Castillo, C. (2004). Adsorption of organic molecules from aqueous solutions on carbon materials. *Carbon, 42*, 83–94.

Moreno-Castillo, C., Rivera-Utrilla, J., Lopez-Ramon, M. V., & Crresco-Marin, F. (1995). Adsorption of some substituted phenols on activated carbons from a bituminous coal. *Carbon, 33*, 845–851.

Mozammel, H. M., Masahiro, O., & Bhattacharya, S. C. (2002). Activated charcoal from coconut shell using $ZnCl_2$ activation. *Biomass Bioenergy, 22*, 397–400.

Namane, A., Mekarzia, A., Benrachedi, K., Bensemra, N., & Hellal, A. (2005). Determination of the adsorption capacity of activated carbon made from coffee grounds by chemical activation with $ZnCl_2$ and $H_3PO_4$. *Journal of Hazardous Material, 119*, 189–194.

Olorundare, O. F., Krause, R. W. M., Okonkwo, J. O., & Mamba, B. B. (2012). Potential application of activated carbon from maize tassel for the removal of heavy metals in water. *Journal of Physics Chemistry of the Earth, 50–52*, 104–110.

Parra, J. B., Sousa, J. C., Pis, J. J., Pajares, J. A., & Bansal, R. C. (1995). Effect of gasification on the porous characteristics of activated carbons from semi anthracite. *Carbon, 33*, 801–807.

Prahas, D., Kartika, Y., Indraswati, N., & Ismadji, S. (2008). Activated carbon from jackfruit peel waste by $H_3PO_4$ chemical activation: pore structure and surface chemistry characterization. *Chem Eng J, 140*, 32–42.

Puziy, A. M., Poddubnaya, O. I., Mart´ınez-Alonso, A., Su´arez-Garc´ıa, F., & Tasc´on, J. M. D. (2005). Surface chemistry of phosphorus-containing carbons of lignocellulosic origin. *Carbon, 43*, 2857–2868.

Rodriguez-Reinoso, F., & Molina-Sabio, M. (1992). Activated carbons from lignocellulosic materials by chemical and/or physical activation: an overview. *Carbon, 30*, 1111–1118.

Ruland, W., & Smarsly, B. (2002). X-ray scattering of non-graphitic carbon: an improved method of evaluation. *Journal of Applied Crystallography, 35*, 624–633.

Sekar, M., Sakthi, V., & Rengaraj, S. (2004). Kinetics and equilibrium adsorption study of lead (II) onto activated carbon prepared from coconut shell. *Journal of Colloid Interface Science, 279*, 307–313.

Srinivasakannan, C., & Bakar, M. Z. A. (2004). Production of activated carbon from rubber wood sawdust. *Biomass Bioenergy, 27*, 89–96.

Srivastava, V. C., Swamy, M. M., Mall, I. D., Prasad, B., & Mishra, I. M. (2006). Adsorptive removal of phenol by bagasse fly ash and activated carbon: equilibrium, kinetics and thermodynamics. *Colloids. Surface A: Physicochemical Engineering Aspects, 272*, 89–104.

Sudaryanto, Y., Hartono, S. B., Irawaty, W., Hindarso, H., & Ismadji, S. (2006). High surface area activated carbon prepared from cassava peel by chemical activation. *Bioresour Technol, 97*, 734–739.

Teng, H., Yeh, T. S., & Hsu, L. H. (1998). Preparation of activated carbon from bituminous coal with phosphoric acid activation. *Carbon, 36*, 1387–1395.

Timur, S., Kantarli, I. C., Ikizoglu, E., & Yanik, J. (2006). Preparation of activated carbons from *oreganum* stalks by chemical activation. *Energy Fuels, 20*, 2636–2641.

Vernersson, T., Bonelli, P. R., Cerrella, E. G., & Cukierman, A. L. (2001). *Arundo donax* cane as a precursor for activated carbons preparation by phosphoric acid activation. *Bioresour Technol, 83*, 95–104.

Wang, T., Tan, S., & Liang, C. (2009). Preparation and characterization of activated carbon from wood via microwave-induced $ZnCl_2$ activation. *Carbon, 47*, 1880–1883.

Wang, L., Guo, Y., Zou, B., Rong, C., Ma, X., Qu, Y., Li, Y., & Wang, Z. (2011). High surface area porous carbons prepared from hydrochars by phosphoric acid activation. *Bioresour Technol, 102*, 1947–1950.

Zvinowanda, C. M., Okonkwo, O. J., Agyei, N. M., & Shabalala, P. N. (2008a). Preparation and characterization of biosorbents made from maize tassel. *Canadian Journal Pure Applied Science, 2*(3), 483–488.

Zvinowanda, C. M., Okonkwo, J. O., Mpangela, V., Phaleng, J., Shabalala, P. N., Dennis, T., Forbes, P., Agyei, N. A., & Ozoemena, K. I. (2008b). Biosorption of toxic metals: the potential use of maize tassel for the removal of Pb (II) from aqueous solutions. *Fresenius Environmental Bulletin, 17*(7a), 814–818.